

The Insulating Nature of Na_2IrO_3 : Mott-type or Slater-type?

Minjae Kim,* Beom Hyun Kim,[†] and B. I. Min[‡]

Department of Physics, PCTP, Pohang University of Science and Technology, Pohang, 790-784, Korea
(Dated: March 5, 2022)

We have investigated temperature-dependent electronic structures of Na_2IrO_3 to unravel its insulating nature. Employing the combined scheme of the density-functional theory (DFT) and the dynamical mean-field theory (DMFT), we have shown that the insulating state persists even above the Néel temperature (T_N), which reveals that Na_2IrO_3 is classified into a Mott-type insulator. The measured photoemission spectrum in the paramagnetic (PM) state is well described by the electronic structure obtained from the DFT+DMFT for the insulating state above T_N . The analysis of optical conductivity, however, suggests that the non-local correlation effect is also important in Na_2IrO_3 . Therefore, Na_2IrO_3 is not to be a standard Mott insulator in that the extended nature and the non-local correlation effect of Ir $5d$ electrons are important as well in describing its electronic and magnetic properties.

PACS numbers: 75.47.Lx, 71.20.-b, 71.70.Ej

Identifying the insulating nature of transition metal oxides has been a central and long-standing subject in modern condensed matter physics.[1] Recent attention has been paid to $5d$ transition metal oxides, Sr_2IrO_4 and Na_2IrO_3 , whether they belong to Mott-type or Slater-type insulators. The strong spin-orbit coupling (SOC) and the rather weak Coulomb correlation of $5d$ electrons are known to be two essential ingredients in determining the ground state physics of Sr_2IrO_4 and Na_2IrO_3 . [2–21] Despite intense studies on the role of interplay between Coulomb interaction and SOC, however, there has been no consensus on the nature of their insulating states yet. For example, on the insulating nature of Sr_2IrO_4 , there exist two contradictory reports, Mott insulator [6] vs. Slater insulator. [7] A marginal Mott insulating state was also proposed, in which the insulating state above the Néel temperature ($T_N=240$ K) was attributed to the presence of short range antiferromagnetic (AFM) correlation. [9, 15] For Na_2IrO_3 too, which is a system of our present interest, there have been debates on its insulating nature. [11–14, 17–21]

Na_2IrO_3 exhibits insulating state at room temperature (T), well above $T_N=15$ K. [11, 12] The paramagnetic (PM) state with Curie-Weiss susceptibility behavior was confirmed up to $T = 500$ K. [12] The zigzag-type AFM ordering occurs below T_N . [8, 22] To explain the AFM insulating ground state of Na_2IrO_3 , both the Mott-type [11, 17] and Slater-type [13, 18, 19, 21] mechanisms of the metal-insulator transition were invoked. In the former, the good basis to describe the local electronic structure is derived by consideration of the on-site atomic SOC and the crystal field. This basis is usually very close to the relativistic $J_{eff}=1/2$ orbital. [5, 16, 20, 23, 24] Superexchange-based formalism is used to describe the zigzag-type AFM ordering. [14, 25] The observed PM insulating state well above T_N supports the Mott-type mechanism. [11] In the Mott-type mechanism, however, very long range magnetic interaction or very high en-

ergy excitation is required to describe the zigzag-type AFM ordering, which raises the question on the validity of superexchange-based formalism. [19] On the other hand, in the Slater-type mechanism, the quasi-molecular orbital (QMO) has been suggested as a good basis with consideration of the strong anisotropic hybridization between $5d$ orbitals of neighboring Ir atoms. [13] The zigzag-type AFM ordering occurs as a consequence of the energy gain from the gap opening at the zone boundary. [18, 21] The Coulomb correlation of $5d$ electrons is considered just to enhance the band gap. Larger extension of $5d$ orbital and multi-peak features in photoemission spectrum (PES) and optical conductivity seem to support the Slater-type mechanism. However, in the Slater-type mechanism, it is hard to explain the observed PM insulating state well above T_N . Therefore, the issue is whether the local AFM ordering is essential in describing the insulating state of Na_2IrO_3 or not.

In this letter, we have investigated T -dependent electronic structures and magnetic properties of Na_2IrO_3 , using the combined scheme of the density functional theory (DFT) and the dynamical mean-field theory (DMFT), [26, 27] and unraveled its insulating nature. We have shown that Na_2IrO_3 at room T has the electronic structure of the PM insulating state, revealing that Na_2IrO_3 is a Mott-type insulator. Highly incoherent PES for Na_2IrO_3 in the PM state is well described by the DMFT incorporating the local dynamical correlation. However, we have also found evidences that Na_2IrO_3 deviates from standard Mott insulators due to extended nature of Ir $5d$ orbitals. The onset of the zigzag-type AFM ordering induces the significant redistribution of charge and spin densities with respect to those of $J_{eff}=1/2$ orbital. This feature implies that, even though Na_2IrO_3 is classified into a Mott-type insulator, the superexchange-based theory assuming the rigid charge degree of freedom needs to be refined to elucidate the magnetic ordering in Na_2IrO_3 . Moreover, optical conductivity, which corre-

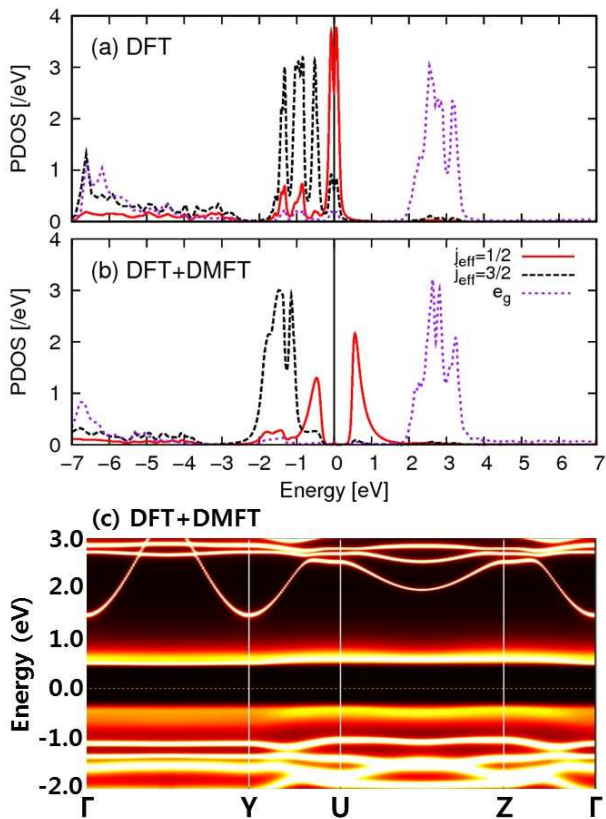


FIG. 1: (Color online) Ir $5d$ partial density of states (PDOS) of Na_2IrO_3 from the DFT (a), and the DFT+DMFT at $T = 300$ K (b). Red solid, black dashed, and purple dotted lines represent $j_{eff}=1/2$, $j_{eff}=3/2$, and e_g projected PDOSs, respectively. See the text for numerical $j_{eff}=1/2$, $j_{eff}=3/2$, and e_g basis. (c) The spectral function from the DFT+DMFT at $T = 300$ K. High symmetry points of Brillouin zone are presented in the Supplemental Material.[34]

sponds to two-particle property, is not well described by the DMFT incorporating only the local dynamical correlation. Thus, the additional non-local spatial electronic correlation is expected to be important to describe optical conductivity in Na_2IrO_3 .

We have performed the fully charge self-consistent DFT+DMFT calculations based on the projection-embedding scheme.[28, 29]. Correlated Ir $5d$ electrons were treated dynamically by the DMFT local self-energy, while s and p electrons were treated on the DFT level. The SOC in the Ir $5d$ orbital is included in all the calculations. For Coulomb interaction parameters, U and J , we employed $U=3.5$ eV and $J=0.8$ eV for the DFT+DMFT. These parameters yield the band gap and PES spectrum in good agreement with the experiment. The DFT part calculation was done by using the full-potential linearized augmented plane wave (FLAPW) band method.[30, 31] For the DFT+DMFT calculation, $T = 300$ K was chosen, and the PM state is assumed. We adopted experimental crystal structure of Na_2IrO_3 . [8] We used numer-

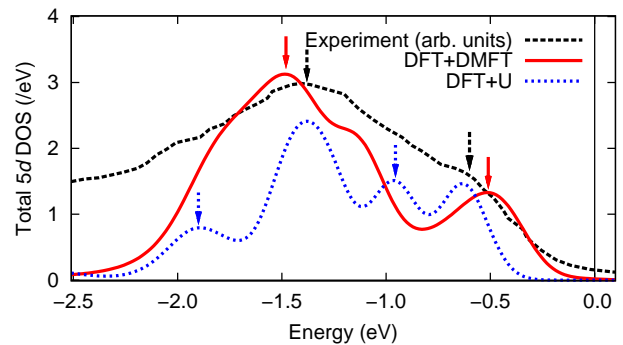


FIG. 2: (Color online) Ir $5d$ PES at $T = 130$ K (black dashed)[11] is compared with calculated PDOSs in the DFT+ U ($U = 2.75$ eV) and the DFT+DMFT ($T = 300$ K). Blue dotted and red solid lines represent the DFT+ U and the DFT+DMFT PDOSs, respectively, which are broadened with a Gaussian function (0.10 eV FWHM). The Fermi level is adjusted in the case of DFT+ U to fit the experiment. Red solid and black dashed arrows point at two dominating peaks in the DFT+DMFT and the measured PES, respectively. Blue dotted arrows point at extra peaks in the DFT+ U , which become significantly broadened in the DFT+DMFT due to the correlation-induced incoherency.

ical $j_{eff}=1/2$, $j_{eff}=3/2$, and e_g bases for Ir $5d$ electrons in the DFT+DMFT, which diagonalize the infinite frequency hybridization function $\Delta(\omega = \infty)$ in the local impurity Green's function of the DMFT result. As shown below, these j_{eff} bases are consistent with relativistic J_{eff} projectors for t_{2g} orbitals in the cubic symmetry.[16, 17] In comparison, we have also performed the DFT and DFT+ U calculations.[32] For the DFT+ U , we used $U = 2.75$ eV and $J = 0.6$ eV, following the existing calculation.[33] We assumed, for the magnetic structure, the observed zigzag-type AFM ordering.[8, 22] See the Supplemental Material (SM) for computational details.[34]

Figure 1(a) and (b) presents partial density of states (PDOS) of $j_{eff}=1/2$, $j_{eff}=3/2$, and e_g states in the DFT and the DFT+DMFT, respectively. The PDOS in the DFT in Fig. 1(a) shows six peaks in the t_{2g} part. Due to anisotropic solid environment in Na_2IrO_3 , the effective orbital degeneracy in the t_{2g} manifold is seen to be well lifted. Mazin *et al.*[13] interpreted these six peaks as the QMOs resulting from strong intra- and weak inter-hexagon hybridizations. On the other hand, in the two uppermost t_{2g} -driven bands, $j_{eff}=1/2$ orbital (red solid) has main contribution with a small amount of $j_{eff}=3/2$ (black dot) contribution. These QMO-driven six peaks and dominant contribution from $j_{eff}=1/2$ near E_F are consistent with previous experimental and theoretical reports.[16, 17, 19] The metallic PDOS in the DFT is not consistent with the insulating ground state of Na_2IrO_3 .

The PDOS in the DFT+DMFT in Fig. 1(b) shows clear Mott gap of ~ 400 meV size in the $j_{eff}=1/2$ states near E_F , as is consistent with experiment.[11] Note that

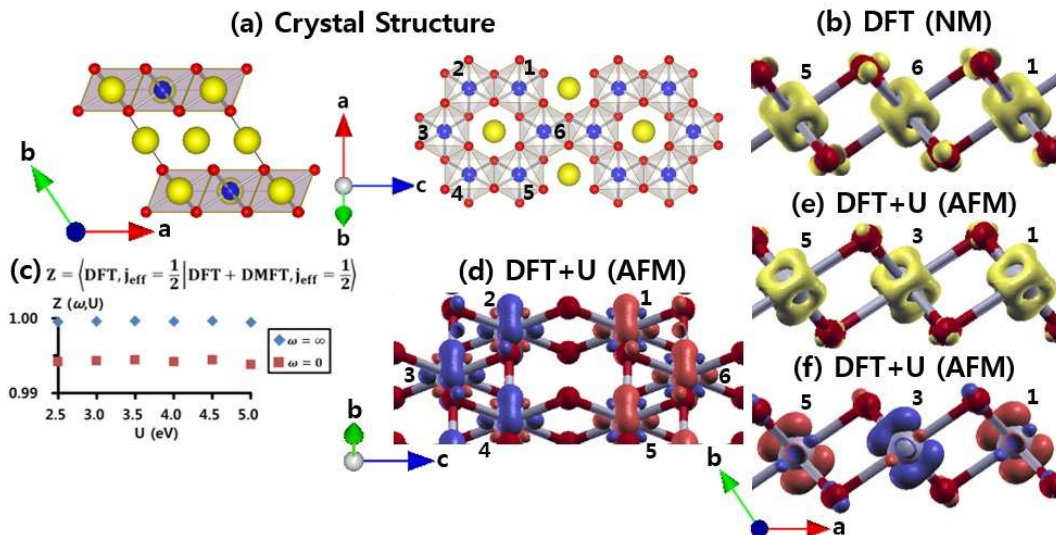


FIG. 3: (Color online) (a) Crystal structure of Na₂IrO₃ (side view in the left and top view in the right).[8] Blue, yellow, and red balls correspond to Ir, Na, and O atoms, respectively. Numbers (1–6) in the top view are given to Ir atoms, for which spin and charge densities are plotted in (b), (d), (e)-(f). (b) The charge density plot of the unoccupied Ir *t*_{2g} band of the nonmagnetic (NM) state in the DFT. Red balls represent oxygen atoms. (c) Projection (Z) between numerical $j_{eff}=1/2$ bases in the DFT and the DFT+DMFT at $\omega=0$, and $\omega=\infty$ with variation of U . (d) The spin density plot of zigzag-type AFM state in the DFT+ U ($U = 2.75$ eV). The obtained spin up (blue) and down (red) densities, respectively, for 2,3,4 and 1,6,5 Ir atoms in the hexagon are consistent with the zigzag-type AFM state. (e) The charge density plot of the unoccupied Ir *t*_{2g} band of zigzag-type AFM state in the DFT+ U ($U = 2.75$ eV). (f) The spin density plot of zigzag-type AFM state in the DFT+ U ($U = 2.75$ eV) (different view from (d)). Isosurfaces are chosen as 0.020 (e/a.u.³) for charge densities, and 0.015 (e/a.u.³) for spin densities.

the DFT+DMFT calculation was done for the PM state (not AFM state) at $T = 300$ K well above $T_N=15$ K. Therefore, the gap opens not due to the AFM cell-doubling but due to the Coulomb correlation effect. This result demonstrates that Na₂IrO₃ can be classified into a Mott-type insulator. This Mott insulating state of Na₂IrO₃ well above T_N is different from the suggested marginal Mott insulating state for Sr₂IrO₄.^[15] It is also noteworthy in Fig. 1(b) that, due to the correlation-induced imaginary part of the dynamical self-energy, *t*_{2g}-driven PDOSs in the DFT+DMFT are significantly broadened with respect to those in the DFT.

The correlation-induced band gap and incoherent features are more clearly seen in the spectral function plot in Fig. 1(c). As shown in the Supplemental Material,^[34] the spectral function becomes more and more incoherent with increasing U , which clearly indicates that the incoherent feature is induced by the correlation effect. It is also notable that the incoherent feature is more prominent for $j_{eff}=1/2$ than for $j_{eff}=3/2$ states.

The correlation-induced incoherence in the DFT+DMFT is essential to describe the measured PES of Na₂IrO₃. In Fig. 2, Ir 5*d* dominant PES near E_F is compared with Ir 5*d* PDOS obtained from both the DFT+ U and the DFT+DMFT. In the PES, there seem to be two dominating peaks, which are significantly broadened.^[11] Our DFT+DMFT result

shows the pronounced two peaks that are broadened by the correlation-induced incoherence. This dynamical correlation-induced incoherence feature is consistent with previous report on Na₂IrO₃,^[23] which analyzed the PES spectra based on the model Hamiltonian. It is also shown in Fig. 2 that, the DFT+ U with static correlation yields four peaks, which is not consistent with the measured PES.

When describing the magnetic interaction in the Mott insulating state of Na₂IrO₃, the charge distribution of *t*_{2g}-driven unoccupied state is usually considered as a rigid object, which is determined by local interactions such as the crystal field and the SOC.^[5, 14, 25] We have confirmed that onset of the zigzag-type AFM ordering induces the significant redistribution of the unoccupied Ir *t*_{2g} state, while the local dynamical correlation in the PM state does not induce the redistribution. Figure 3 illustrates this argument. In Fig. 3(b), the charge density of the unoccupied Ir *t*_{2g} band in the DFT is plotted. The cubic-shaped charge density indicates the dominant $J_{eff}=1/2$ character of the band. Figure 3(c) presents the projection $Z(\omega, U)$ between numerical $j_{eff}=1/2$ bases in the DFT and the DFT+DMFT with varying U . $j_{eff}=1/2$ bases were obtained from the diagonalization of the hybridization function at zero and infinite frequency ($\Delta(0)$ and $\Delta(\infty)$), with and without considering the self-energy contribu-

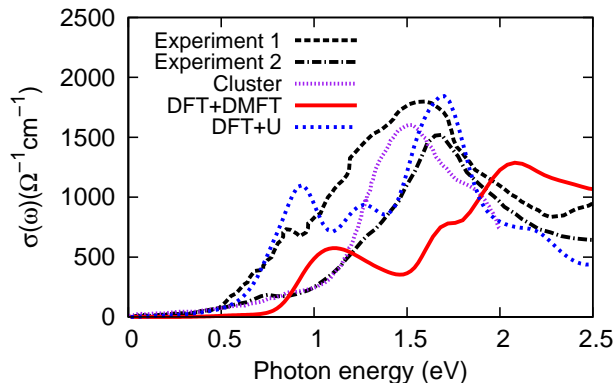


FIG. 4: (Color online) Experimental optical conductivities $\sigma(\omega)$'s of Na_2IrO_3 at $T = 300$ K, Exp 1 from Ref. [11] and Exp 2 from Ref.[17], are compared with calculated optical conductivities using the DFT+DMFT, the DFT+ U ($U = 2.75$ eV), and four-site cluster multiplet calculations.[20]

tion for the DFT+DMFT and the DFT, respectively. $j_{eff}=1/2$ orbital for $\omega = \infty$ is relevant to the single ion anisotropy, while $j_{eff}=1/2$ orbital for $\omega = 0$ is relevant to the low energy electronic excitation.[15, 35] As shown in Fig.3(c), $Z(\omega, U)$ is nearly constant with respect to the variation of U , and close to 1 for $\omega = \infty$ and 0.995 for $\omega = 0$. This result implies that numerical $j_{eff}=1/2$ bases of the DFT and the DFT+DMFT resemble each other. Namely, the local correlation does not affect the charge distribution, and so the DFT+DMFT has similar charge distribution of unoccupied t_{2g} -driven band to that of the DFT.

On the other hand, the onset of the zigzag-type AFM ordering induces significant elongation of charge density along the ferromagnetic chain direction, as shown in Fig. 3(e) for the DFT+ U result. Spin densities in Fig. 3(d) and (f) also verify this phenomenon. In the $J_{eff}=1/2$ basis, the spin densities from three different orbitals in the t_{2g} manifold have equal up, up, and down spin contributions. In our DFT+ U results with the zigzag-type AFM ordering, the orbital component directed normal to the ferromagnetic chain is much smaller than other two orbital components directed along the ferromagnetic chain. As a result, the ratio between orbital and spin moment ($\mu_L/\mu_S=1.59$ with $\mu_{tot}=0.70 \mu_B$) deviates largely from the ideal $J_{eff}=1/2$ case of $\mu_L/\mu_S=2$. This feature indicates that there will be significant redistribution of charge in the AFM transition due to the extended nature of Ir $5d$ orbital,[36] which is not expected for the superexchange-based magnetic interaction in the normal Mott insulating state.

In Fig. 4, experimental optical conductivities $\sigma(\omega)$'s are compared with computed optical conductivities from the DFT+DMFT, the DFT+ U , and four-site cluster multiplet calculations.[20] In experiments, only one peak is dominant in the optical spectrum.[11, 17] In the DFT+ U , there occur two main peaks, as in previous

DFT+ U calculation,[33] which does not seem to be consistent with experiments. The peak near 0.75 eV should be suppressed. In the DFT+DMFT, the peak near 0.75 eV is significantly suppressed due to the incoherency from the local self-energy. However, overall peaks are shifted upward and the main peak position (~ 2 eV) is not consistent with the experimental main peak position (~ 1.5 eV). If we use smaller U in the DFT+DMFT, the main peak position is matched but the peak near 0.75 eV is not suppressed, and so the resulting $\sigma(\omega)$ becomes similar to that of the DFT+ U (see the SM).[34] The inconsistent DFT+DMFT result suggests that the local dynamical correlation is not sufficient to describe optical conductivity of Na_2IrO_3 , which corresponds to a two-particle property.

In contrast, the optical conductivity from the four-site cluster multiplet calculation seems to be well consistent with experiments, suggesting the importance of the non-local correlation effect in Na_2IrO_3 . [20] Similar feature was found in cuprate too, for which PES that is single particle property is well described by the single-site DMFT, but optical conductivity that is two-particle property is described only by the cluster DMFT calculation.[37] Thus, it is expected that the non-local correlation effect would be important for optical conductivity due to the extended nature of Ir $5d$ orbital in Na_2IrO_3 . More systematic study of cluster-size dependency of the optical spectrum would be an interesting future subject.

In conclusion, we show that Na_2IrO_3 is a Mott-type insulator. Differently from Sr_2IrO_4 , the Mott insulating state persists in the PM state well above T_N . The local correlation-induced incoherence in this Mott insulating phase explains the measured PES spectrum of Na_2IrO_3 well. Yet, due to the extended nature of $5d$ orbital, the insulating nature of Na_2IrO_3 is different from that of a standard Mott insulator. The onset of AFM ordering induces significant redistribution of charge. The analysis of optical conductivity suggests that the non-local correlation effect also plays a role in Na_2IrO_3 . Therefore, our results indicate that Na_2IrO_3 has the Mott-type insulating nature, but the itineracy of the charge degree of freedom and the non-local correlation effect should also be taken into account to describe physical properties of this system having localized and itinerant duality of $5d$ electrons.

Helpful discussions with C.-J. Kang are greatly appreciated. This work was supported by the POSTECH BK21+ Physics Project, Max-Planck POSTECH/KOREA Research Initiative, and the KISTI supercomputing center (No. KSC-2014-C3-044).

* Present address: Collège de France, 75005 Paris, France

[†] Present address: RIKEN, Saitama 351-0198, Japan

[‡] Electronic address: bimin@postech.ac.kr

- [1] M. Imada, A. Fujimori, and Y. Tokura, *Rev. of Mod. Phys.* **70**, 1039 (1998).
- [2] B. J. Kim, H. Jin, S. J. Moon, J.-Y. Kim, B.-G. Park, C. S. Leem, J. Yu, T. W. Noh, C. Kim, S.-J. Oh, J.-H. Park, V. Durairaj, G. Cao, and E. Rotenberg, *Phys. Rev. Lett.* **101**, 076402 (2008).
- [3] B. J. Kim, H. Ohsumi, T. Komesu, S. Sakai, T. Morita, H. Takagi, and T. Arima, *Science* **323**, 1329 (2009).
- [4] H. Jin, H. Jeong, T. Ozaki, and J. Yu, *Phys. Rev. B* **80**, 075112 (2009).
- [5] G. Jackeli, and G. Khaliullin, *Phys. Rev. Lett.* **102**, 017205 (2009).
- [6] C. Martins, M. Aichhorn, L. Vaugier, and, S. Biermann, *Phys. Rev. Lett.* **107**, 266404 (2011).
- [7] R. Arita, J. Kuneš, A. V. Kozhevnikov, A. G. Eguiluz, and M. Imada, *Phys. Rev. Lett.* **108**, 086403 (2012).
- [8] S. K. Choi, R. Coldea, A. N. Kolmogorov, T. Lancaster, I. I. Mazin, S. J. Blundell, P. G. Radaelli, Y. Singh, P. Gegenwart, K. R. Choi, S.-W. Cheong, P. J. Baker, C. Stock, and J. Taylor, *Phys. Rev. Lett.* **108**, 127204 (2012).
- [9] S. Fujiyama, H. Ohsumi, T. Komesu, J. Matsuno, B. J. Kim, M. Takata, T. Arima, and H. Takagi, *Phys. Rev. Lett.* **108**, 247212 (2012).
- [10] B. H. Kim, G. Khaliullin, and B. I. Min, *Phys. Rev. Lett.* **109**, 167205 (2012).
- [11] R. Comin, G. Levy, B. Ludbrook, Z.-H. Zhu, C. N. Venstra, J. A. Rosen, Y. Singh, P. Gegenwart, D. Stricker, J. N. Hancock, D. van der Marel, I. S. Elfimov, and A. Damascelli, *Phys. Rev. Lett.* **109**, 266406 (2012).
- [12] Y. Singh, and P. Gegenwart, *Phys. Rev. B* **82**, 064412 (2010).
- [13] I. I. Mazin, H. O. Jeschke, K. Foyevtsova, R. Valentí, and D. I. Khomskii, *Phys. Rev. Lett.* **109**, 197201 (2012).
- [14] J. Chaloupka, G. Jackeli, and G. Khaliullin, *Phys. Rev. Lett.* **110**, 097204 (2013).
- [15] H. Zhang, K. Haule, and D. Vanderbilt, *Phys. Rev. Lett.* **111**, 246402 (2013).
- [16] H.-S. Kim, C. H. Kim, H. Jeong, H. Jin, and J. Yu, *Phys. Rev. B* **87**, 165117 (2013).
- [17] C. H. Sohn, H.-S. Kim, T. F. Qi, D. W. Jeong, H. J. Park, H. K. Yoo, H. H. Kim, J.-Y. Kim, T. D. Kang, D.-Y. Cho, G. Cao, J. Yu, S. J. Moon, and T. W. Noh, *Phys. Rev. B* **88**, 085125 (2013).
- [18] I. I. Mazin, S. Manni, K. Foyevtsova, H. O. Jeschke, P. Gegenwart, and R. Valentí, *Phys. Rev. B* **88**, 035115 (2013).
- [19] K. Foyevtsova, H. O. Jeschke, I. I. Mazin, D. I. Khomskii, and R. Valentí, *Phys. Rev. B* **88**, 035107 (2013).
- [20] B. H. Kim, G. Khaliullin, and B. I. Min, *Phys. Rev. B* **89**, 081109(R) (2014).
- [21] H.-J. Kim, J.-H. Lee, and J.-H. Cho, *Sci. Rep.* **4**, 5253 (2014).
- [22] F. Ye, S. Chi, H. Cao, B. C. Chakoumakos, J. A. Fernandez-Baca, R. Custelcean, T. F. Qi, O. B. Korneta, and G. Cao, *Phys. Rev. B* **85**, 180403(R) (2012).
- [23] F. Trouselet, M. Berciu, A. M. Oleś, and P. Horsch, *Phys. Rev. Lett.* **111**, 037205 (2013).
- [24] H. Gretarsson, J. P. Clancy, X. Liu, J. P. Hill, E. Bozin, Y. Singh, S. Manni, P. Gegenwart, J. Kim, A. H. Said, D. Casa, T. Gog, M. H. Upton, H.-S. Kim, J. Yu, V. M. Katukuri, L. Hozoi, J. van den Brink, and Y.-J. Kim, *Phys. Rev. Lett.* **110**, 076402 (2013).
- [25] Y. Yamaji, Y. Nomura, M. Kurita, R. Arita, and M. Imada, *Phys. Rev. Lett.* **113**, 107201 (2014).
- [26] A. Georges, G. Kotliar, W. Krauth, and M. J. Rozenberg, *Rev. Mod. Phys.* **68**, 13 (1996).
- [27] G. Kotliar, S. Y. Savrasov, K. Haule, V. S. Oudovenko, O. Parcollet, and C. A. Marianetti, *Rev. Mod. Phys.* **78**, 865 (2006).
- [28] K. Haule, C.-H. Yee, and K. Kim, *Phys. Rev. B* **81**, 195107 (2010).
- [29] K. Haule, *Phys. Rev. B* **75**, 155113 (2007).
- [30] M. Weinert, E. Wimmer, and A. J. Freeman, *Phys. Rev. B* **26**, 4571 (1982).
- [31] P. Blaha, K. Schwarz, G.K.H. Madsen, D. Kvasnicka, J. Luitz, WIEN2k (Karlheinz Schwarz, Technische Universität Wien, Austria, 2001).
- [32] V. I. Anisimov, I. V. Solovyev, M. A. Korotin, M. T. Czyzyk, and G. A. Sawatzky, *Phys. Rev. B* **48**, 16929 (1993).
- [33] Y. Li, K. Foyevtsova, H. O. Jeschke, and R. Valentí, *Phys. Rev. B* **91**, 161101(R) (2015).
- [34] See the Supplementary Material for (i) Brillouin zone, and (ii) U dependence of electronic structure, PES, and optical conductivity in the DFT+DMFT.
- [35] T. Birol, and K. Haule, *Phys. Rev. Lett.* **114**, 096403 (2015).
- [36] Strongly distorted spin density from ideal $J_{eff}=1/2$ orbital in Ref. [21] is similar to our results in Fig. 3(d) and (f). Our choice of isosurface electron density is nearly 25 times larger than that in Ref. [21], and so our isosurface is less sensitive to the redistribution of charge than that in Ref.[21] Thus, captured distortions of charge and spin densities in our results indicate significant redistribution of electron density with onset of the zigzag-type AFM ordering.
- [37] A. Go, and A. J. Millis, *Phys. Rev. Lett.* **114**, 016402 (2015).